



Published in final edited form as:

Nat Commun. ; 5: 5601. doi:10.1038/ncomms6601.

Cell cycle-linked MeCP2 phosphorylation modulates adult neurogenesis involving the Notch signaling pathway

Hongda Li^{1,2}, Xiaofen Zhong¹, Kevin Fongching Chau¹, Nicholas J. Santistevan³, Weixiang Guo⁴, Guangyao Kong⁵, Xuekun Li⁶, Mitul Kadakia¹, Jamie Masliah¹, Jingyi Chi¹, Peng Jin⁷, Jing Zhang⁴, Xinyu Zhao¹, and Qiang Chang^{1,2,8,*}

¹Waisman Center, University of Wisconsin-Madison, USA

²Genetics Training Program, University of Wisconsin-Madison, USA

³University of New Mexico, USA

⁴State Key Laboratory of Molecular Developmental Biology, Institute of Genetics and Developmental Biology, Chinese Academy of Sciences, China

⁵McArdle Laboratory, University of Wisconsin-Madison, USA

⁶Institute of Genetics, College of Life Sciences, Zhejiang University, China

⁷Emory University, USA

⁸Department of Neurology, University of Wisconsin-Madison, USA

Abstract

Neuronal activity regulates the phosphorylation states at multiple sites on MeCP2 in postmitotic neurons. The precise control of the phosphorylation status of MeCP2 in neurons is critical for the normal development and function of the mammalian brain. However, it is unknown whether phosphorylation at any of the previously identified sites on MeCP2 can be induced by signals other than neuronal activity in other cell types, and what functions MeCP2 phosphorylation may have in those contexts. Here we show that, in neural progenitor cells isolated from the adult mouse hippocampus, cell cycle-linked phosphorylation at serine 421 on MeCP2 is directly regulated by aurora kinase B, and modulates the balance between proliferation and neural differentiation through the Notch signaling pathway. Our findings suggest MeCP2 S421 phosphorylation may function as a general epigenetic switch accessible by different extracellular stimuli through different signaling pathways for regulating diverse biological functions in different cell types.

Users may view, print, copy, and download text and data-mine the content in such documents, for the purposes of academic research, subject always to the full Conditions of use:http://www.nature.com/authors/editorial_policies/license.html#terms

*Correspondence should be addressed to: Qiang Chang, qchang@waisman.wisc.edu.

Author Contributions

Q.C. directed the studies. H.L., J.Z., P.J., X-Y.Z., and Q.C. conceived and designed the experiments. H.L., X-F.Z., K.F.C., N.J.S., W.G., G.K., X.L., M.K., J.M. and J.C. performed the experiments. The paper was written by Q.C. and H.L., and commented on by all authors.

Competing financial interests

The authors declare no competing financial interests.

Introduction

Methyl-CpG binding protein 2 (MeCP2) is an important reader and interpreter of DNA methylation across the genome¹. Mutations in *MECP2* have been identified as the cause of Rett syndrome (RTT)², a severe neurodevelopmental disorder³. A better understanding of how extracellular signals access MeCP2 to generate adaptive functional outputs will provide valuable insights into how such a critical epigenetic interface influences normal and abnormal development and function of the mammalian nervous system. In postmitotic neurons, depolarization-induced Ca²⁺ influx through voltage-gated calcium channels (VGCCs) has been shown to trigger phosphorylation of MeCP2 at serine 421 (S421)^{4,5}, which is required for regulating synaptogenesis, dendritic morphology, synaptic scaling, long-term potentiation and spatial memory in the adult mouse brain⁶⁻⁸. To date, S421 phosphorylation has only been observed in postmitotic neurons^{5,6,9}.

Adult neurogenesis is a fascinating phenomenon that has attracted a lot of attention in recent years. Research in the field has mainly focused on the function of continued neurogenesis in adult life and the molecular mechanism underlying the process^{10,11}. Evidence is just emerging to suggest a potential role of DNA methylation-dependent epigenetic mechanisms in regulating mammalian adult neurogenesis¹²⁻¹⁵.

In this study, we provide evidence that S421 is phosphorylated in adult neuroprogenitor cells (aNPC) isolated from the mouse hippocampus in response to growth signals. S421 phosphorylation in aNPC is linked to cell cycle and directly regulated by aurora kinase B, and plays a critical role in balancing aNPC proliferation/neural differentiation through the Notch signaling pathway. Our results suggest that, in addition to the precise control of MeCP2 expression level, the regulation of posttranslational modification of MeCP2 is another mechanism underlying adult neurogenesis. In addition, stimulus-induced MeCP2 phosphorylation has the potential to function as a general epigenetic switch for regulating a diverse range of biological functions.

Results

Cell cycle-linked MeCP2 S421 phosphorylation in aNPCs

We discovered that S421 was phosphorylated (Fig. 1a) in proliferating aNPCs isolated from the dentate gyrus (DG) of wild type (WT) mouse hippocampus (Supplementary Fig. 1a). This phosphorylation was abolished in phosphor-mutant aNPCs isolated from the *Mecp2^{S421A;S424A/y}* hippocampus (Fig. 1a). Consistent with our previous report⁶, the level of total MeCP2 protein in aNPCs was indistinguishable between the wild type and the phosphor-mutant (Fig. 1a). When the WT aNPCs were differentiated into neurons, S421 phosphorylation first decreased, but then increased again as the neurons matured (Supplementary Fig. 1b). Since previous studies on postmitotic neurons have identified calcium influx through VGCCs as the trigger for S421 phosphorylation, we first tested whether they are involved in inducing S421 phosphorylation in aNPCs. Neither membrane depolarization by KCl nor treatment by Bay K8644, a calcium channel agonist, induced S421 phosphorylation in aNPCs (Supplementary Fig. 1c). Consistent with these results, Nimodipine, a VGCC blocker, failed to inhibit S421 phosphorylation in aNPCs

(Supplementary Fig. 1d–e). In contrast, roscovitine, a broad-spectrum inhibitor of cyclin-dependent kinases (CDKs), significantly decreased S421 phosphorylation in aNPCs (Supplementary Fig. 1d–e). In light of this surprising result and the fact that aNPCs are dividing cells, we explored the possibility that growth factor and cell cycle regulation are involved in regulating S421 phosphorylation. Withdrawing growth factors led to concurrent decrease of phosphorylation of S421 (Fig. 1b–c) and absence of G2/M phase cells (Supplementary Fig. 2a) in WT aNPCs. These alterations were unlikely to be secondary to potential cell fate changes, because expression of key cell type markers remained similar before and after the withdrawal of growth factors (Supplementary Fig. 2b–c). To investigate whether S421 phosphorylation is linked to cell cycle, we arrested WT aNPCs at the G2/M phase with nocodazole (Supplementary Fig. 2d–e) or colchicine and observed a dramatic increase in the level of phospho-S421 (Fig. 1d,f and Supplementary Fig. 2f). Using a series of pharmacological reagents, we excluded the involvement of VGCCs, CaMKK and CaMKII in regulating cell cycle-linked S421 phosphorylation in aNPCs, because selective inhibitors of VGCCs, CaMKK or CaMKII failed to block cell cycle-linked S421 phosphorylation in these cells (Supplementary Fig. 2g). In contrast, roscovitine, a synthetic molecule with sub- μ M IC50 values against CDK1, CDK2, CDK5, CDK7 and CDK9¹⁶, was highly effective in blocking nocodazole-induced S421 phosphorylation, suggesting that cell cycle dependent kinases (CDKs) were upstream of S421 phosphorylation in aNPCs (Fig. 1e–f). Since nocodazole and roscovitine together arrested slightly more cells at G1 than nocodazole alone (Supplementary Fig. 2d–e), roscovitine may have additional indirect effect on S421 phosphorylation through cell cycle alteration. Finally, such cell cycle-linked MeCP2 S421 phosphorylation was also observed in aNPCs isolated from the subventricular zone (SVZ) and NPCs isolated from neonatal brains (Supplementary Fig. 2h), raising the possibility that this may be a general phenomenon in proliferating cells.

Aurora kinase B directly phosphorylates MeCP2 S421 in aNPCs

Since the consensus sequence for the phosphorylation site of a CDK substrate, [serine/threonine]-proline-any amino acid-[lysine/arginine], is not found around S421, CDKs are unlikely to be the direct kinase for S421 in aNPCs. To search for the kinase that is directly responsible for phosphorylating S421 in aNPCs, we performed an *in silico* screen of consensus substrate sequences to identify a list of potential kinases, which was followed by a pharmacological screen in nocodazole-treated N2A cells. Aurora kinase B was the only candidate coming out of this two-step screen (Supplementary Fig. 2i). Consistent with previous reports that aurora kinase B is upregulated at the G2/M phase and downstream of CDKs^{17,18}, we found that its level increased significantly in nocodazole-treated aNPCs, which was blocked by roscovitine (Fig. 1e). The phosphorylation level of serine 10 on histone 3, a known substrate of aurora kinase B¹⁹, closely followed the changes in the level of aurora kinase B in aNPCs (Fig. 1e). Hesperadin, a highly specific inhibitor of aurora kinase B, efficiently blocked cell cycle-linked S421 phosphorylation in aNPCs (Fig. 2a–b and Supplementary Fig. 2j–k), suggesting the aurora kinase B is required for S421 phosphorylation in these cells. To confirm this finding with an independent method, we generated lentivirus encoding shRNA specific for aurora kinase B (Supplementary Fig. 2l), and found it also significantly blocked cell cycle-linked S421 phosphorylation in aNPCs (Fig. 2c–d). As a negative control, a lentivirus encoding shRNA specific for EGFP had no

effect on aurora kinase B level and S421 phosphorylation in aNPCs (Fig. 2c–d). To test whether MeCP2 and aurora kinase B physically interact with each other, we overexpressed epitope-tagged MeCP2 and aurora kinase B in Neuro2A cells and performed reciprocal co-immunoprecipitation followed by Western blot experiments. We found that flag-tagged aurora kinase B, but not flag-tagged EGFP, could pull down MeCP2 (Fig. 2e). Reversely, flag-tagged MeCP2, but not flag-tagged EGFP, could pull down aurora kinase B (Fig. 2f). Furthermore, the physical interaction between MeCP2 and aurora kinase B, as well as that between aurora kinase B and its known substrate-histone H3, can be detected in aNPCs arrested at the G2/M phase (Fig. 2g). Finally, when purified MeCP2 protein was incubated with aurora kinase B (but not an inactive form of the kinase-AURKB-DN) in the presence of ATP in an *in vitro* kinase assay, S421 was readily phosphorylated (Fig. 2h). Taken together, these results identify aurora kinase B as the direct kinase of MeCP2 S421 phosphorylation in aNPCs.

Altered proliferation/differentiation in phosphor-mutant NPC

To reveal the functional significance of S421 phosphorylation in aNPCs, we examined proliferation and differentiation in both WT and phosphor-mutant aNPCs. Significantly fewer BrdU -labeled Nestin⁺Sox2⁺ (triple positive) aNPCs were observed in phosphor-mutant compared with WT cells (Fig. 3a–b and Supplementary Fig. 3a), indicating a reduced proliferation potential. While the phosphor-mutant aNPCs consistently took more time to grow than the wild type aNPCs at each passage, no significant difference was found in the percentage of cells at each stages of the cell cycle (Supplementary Fig. 3b). Upon differentiation, significantly more Tuj1 or MAP2 positive cells were detected in phosphor-mutant compared with WT cells (Fig. 3c–d and Supplementary Fig. 3c–d), suggesting increased potential in neural differentiation. In contrast, no difference in glial differentiation was observed between the WT and phosphor-mutant aNPCs (Fig. 3e–f). Consistent with the stereological counting data (Fig. 3c–f), the mRNA levels of *Tuj1* and *NeuroD1*, two neuronal genes, were significantly higher in differentiated phosphor-mutant aNPCs than in WT aNPCs; while the mRNA levels of *GFAP*, a glial gene, remained unchanged in these cells (Fig. 3g). To validate our *in vitro* observations, we first performed BrdU labeling (Fig. 3h–i) to mark all the proliferating aNPCs in the subgranular zone of the hippocampus in adult mice, and conducted unbiased stereological quantification throughout the dentate gyrus of the hippocampus to compare the numbers of BrdU labeled cells in the dentate gyrus between *Mecp2*^{S421A;S424A/y} and WT littermates (n=9 in each group). Fewer BrdU labeled cells (89% of WT level) were found in the *Mecp2*^{S421A;S424A/y} hippocampus than in the WT littermate (Fig. 3j, p=0.002, unpaired t-test with Welch's correction). Consistent with the BrdU labeling results, fewer Ki67 (a proliferation marker) stained cells (65% of WT level) were found in the *Mecp2*^{S421A;S424A/y} hippocampus than in the WT littermates in stereological analysis an additional cohort of mice (Fig. 3k, n=6 in each group, p=0.003, unpaired t-test with Welch's correction). In addition to aNPC proliferation, we also examined the cell fates of these adult-born cells 4 weeks after they were born (as illustrated in Fig. 3l). In the study, dividing aNPCs in the hippocampus of 8–9 weeks old *Mecp2*^{S421A;S424A/y} mice (n=9) and their WT littermates (n=8) were first labeled by BrdU and given 4 weeks to differentiate. Sections throughout the hippocampus were triple labeled with an anti-BrdU antibody (to mark adult-born cells), an anti-NeuN antibody (to mark

neurons), and an anti-S100 β antibody (to mark glial cells). Under a confocal microscope, cells were identified as new neurons if they were positive for both BrdU and NeuN (Fig. 3m, indicated by arrows), as new glial cells if they were positive for both BrdU and S100 β (Fig. 3m, indicated by an arrowhead), or as undetermined if they were only positive for BrdU. All BrdU positive cells (407 ± 132 in WT vs. 379 ± 81 in phosphor-mutant, unpaired t-test with Welch's correction, $p=0.85$) in the subgranular zone from all stained sections were included in the analysis. Our results showed that a higher proportion of the dividing aNPCs in the hippocampus of the *Mecp2*^{S421A;S424A/y} mice differentiated into neurons (Fig. 3n, $p=0.01$, unpaired t-test with Welch's correction) at the expense of undetermined cells (Fig. 3n, $p=0.02$, unpaired t-test with Welch's correction). As for the absolute number of BrdU positive newborn neurons, no significant difference was detected between the *Mecp2*^{S421A;S424A/y} mice and their WT littermate (283 ± 86 in WT vs. 299 ± 61 in phosphor-mutant, unpaired t-test with Welch's correction, $p=0.88$). The percentage of glial cells differentiated from the newborn cells in the adult hippocampus did not change significantly in the *Mecp2*^{S421A;S424A/y} mice when compared with the WT littermates (Fig. 3n, $p=0.48$, unpaired t-test with Welch's correction). No difference in the volume of granular cell layer was observed between the WT and phosphor-mutant mice (Supplementary Fig. 3e). Taken together, these *in vitro* and *in vivo* observations consistently identify a critical role of S421 phosphorylation in regulating aNPC proliferation and differentiation.

Notch signaling is downstream of S421 phosphorylation in NPC

To elucidate the molecular mechanism underlying the effect of S421 phosphorylation on balancing aNPC proliferation/neural differentiation, we performed transcription profiling in WT and phosphor-mutant aNPCs using the Neurogenesis and Neural Stem Cells PCR Array (Qiagen). Among the significant transcription changes in phosphor-mutant aNPCs, several belonged to the well-studied Notch signaling pathway (Supplementary Fig. 4a). Thus we expanded our analysis to examine RNA levels of additional components of the Notch pathway, and found consistent decrease in the ligand (*Dll1* and *Jag2*), receptor (*Notch1*) and several target genes (*Hes3*, *Hes5*, *Hey1*, and *Heyl*) of this pathway in phosphor-mutant aNPCs (Fig. 4a–b and Supplementary Fig. 4b). In addition, Western blot results confirmed the significant decrease in DLL1 protein level in phosphor-mutant aNPCs (Fig. 4c–d). As the link between ligand/receptor interaction on the cell membrane and target gene activation in the nucleus²⁰, the intracellular domain of Notch (NICD) was found to be significantly lower in the phosphor-mutant aNPCs (Fig. 4e–f). Consistent with the idea that decreased Notch signaling in phosphor-mutant aNPC may underlie the observed changes in aNPC proliferation/differentiation, treatment of WT aNPCs with a Notch inhibitor led to decreased proliferation and increased neural differentiation similar to those observed in phosphor-mutant aNPCs (Supplementary Fig. 4c–d). Furthermore, we attempted to rescue the proliferation/differentiation phenotypes by overexpressing NICD in these cells. GFP- or NICD-expressing lentiviruses were produced and used to infect either WT or phosphor-mutant aNPCs. While the NICD level in GFP-lentivirus-infected phosphor-mutant aNPCs remained much lower than that in GFP-lentivirus-infected WT aNPCs, the NICD level was similar between NICD-lentivirus-infected phosphor-mutant aNPCs and GFP-lentivirus-infected WT aNPCs (Supplementary Fig. 4e). In addition, overexpression of NICD, but not overexpression of GFP, was sufficient to reverse the reduced transcription of Notch

phenotypes in proliferation/differentiation. The fact that Smrt et al¹² didn't observe any significant change in aNPC proliferation/differentiation in the hippocampus of *Mecp2* null mice is not necessarily inconsistent with our findings in the *Mecp2* phosphor-mutant mice, because other post-translational modifications on the MeCP2 protein may have opposing roles in regulating aNPC proliferation and differentiation. In wild type cells, the two forces balance each other out. In S421A phosphor-mutant cells, the balance is lost and the phenotypes become evident. In *Mecp2* null cells, the opposite regulatory roles of both S421 and the other uncharacterized modifications are lost. Thus no overt aNPC proliferation/differentiation phenotypes could be observed. In addition to affecting neural differentiation, Tsujimura et al¹⁴ also observed changes in glial differentiation when MeCP2 is overexpressed in embryonic neural progenitors. The reason we didn't observe similar changes in glial differentiation either *in vitro* or *in vivo* is likely due to the difference in developmental timing (adult vs. embryonic) and the nature of MeCP2 changes (phosphorylation vs. expression level). In comparing our findings with previous reports, another point worth noting is that the exact mechanism accessed by MeCP2 to regulate neurogenesis may be cell type specific. For instance, microRNAs, such as miR137, have been identified as the downstream effectors of MeCP2 in regulating the proliferation/differentiation of aNPCs isolated from the subventricular zone¹³. However, the level of miR137 expression is extremely low in our hippocampal aNPCs, and is not significantly different between WT and *Mecp2* phosphor-mutant (Supplementary Fig. 4o). Therefore, although we cannot rule out a potential role of other microRNAs, miR137 expression is unlikely to be regulated by S421 phosphorylation and involved in regulating the proliferation/differentiation of hippocampal aNPCs. Moreover, given the wide distribution of MeCP2 across the genome^{7,21} and many of the proteins it interacts to maintain normal cellular functions²²⁻²⁶, Notch signaling is unlikely to be the only misregulated pathway in the *Mecp2* phosphor-mutant aNPCs. Future studies will be needed for a more complete understanding of the molecular events downstream of S421 phosphorylation in these cells. Finally, since both S421 and S424 were mutated in our study, it is a formal possibility that S424A also contributed to the phenotypes observed in the *Mecp2*^{S421A;S424A/y} aNPCs both *in vitro* and *in vivo*. Future studies on the *Mecp2*^{S421A/y} aNPCs and *Mecp2*^{S421A/y} mice are needed to evaluate this possibility.

In summary, our study provides the first evidence that S421 of MeCP2 is phosphorylated in a proliferating cell type and plays a key role in regulating the proliferation and neural differentiation of aNPCs. Moreover, we have identified growth factors and CDKs as the signaling components upstream of S421 phosphorylation and aurora kinase B as the direct kinase for phosphorylating S421 in these cells. Finally, we have revealed Notch signaling as the molecular mechanism underlying the influence of S421 phosphorylation on the balance of proliferation and neural differentiation in these cells. Together with earlier studies on the regulation of S421 phosphorylation and its function in postmitotic neurons, our findings raise the possibility that S421 phosphorylation may function as a general regulatory switch accessible to diverse stimuli acting through distinct signaling pathways with important functional outcomes in different cell types.

Methods

Animals

All the experiments were performed using male mice. *Mecp2*^{S421A;S424A/y} mice have been backcrossed to C57BL/6 background for more than 10 generations. Mice were housed in 12hr light (6am–6pm)/12 hr dark (6pm–6am) cycle. Mice were housed <5 mice/cage. All protocols were approved by the Institutional Animal Care and Use Committee at University of Wisconsin-Madison.

DNA construct

The cDNAs of mouse *Mecp2*, *AurkB*, the intracellular domain of Notch1 (NICD) and EGFP were subcloned to lentiviral expression vector. Sequence encoding the Flag peptide (DYKDDDDK) was introduced to the 3' end of *Mecp2* and *AurkB* cDNA by PCR. Expression of genes is driven by EF-1 Alpha (EF1 α) promoter (pEF1 α vector is a gift from Dr. Su-chun Zhang's lab). The mutation in AurkB-DN (dominant negative, K106R in the putative ATP binding site) cDNA was generated by site-directed mutagenesis PCR.

Lentiviral vector LentiLox 3.7 is used for expression of shRNA against EGFP and *AurkB* (<http://web.mit.edu/jacks-lab/protocols/pll37cloning.htm>). Sense and antisense target sequences of EGFP and *AurkB* were linked by loop sequence TTCAAGAGA and subcloned into LentiLox 3.7. Expression of shRNA is driven by U6 promoter.

EGFP target sequence: gaacggcatcaaggtgaac

AurkB target sequence: ggtaattcacagagacata

Antibodies and drugs

The following primary antibodies were used: Anti-MeCP2 (Cell Signaling, 3456, 1:2,000), Anti-MeCP2 (Abcam, ab50005, 1:2,000), Anti phospho-S421 (custom made by Covance, 1:2,000), anti- β -Actin (Sigma-Aldrich, a5441, 1:5,000), anti-AURKB (Millipore, 04-1036, 1:1,000; Cell Signalling, 3094, 1:1,000), anti-DLL1 (Abcam, Ab84620, 1:1,000), anti-NICD (Cell Signaling, 4147, 1:1,000), anti-phospho-Histone H3 (Ser10) (Cell Signalling, 3377, 1:1,000), anti-Histone H3 (Active Motif, 39163, 1:10,000), anti-S100b (SWANT, 1:500), anti-NeuN (Millipore, MAB377, 1:1,000), anti-BrdU (Accurate Chemical & Scientific, H7786, 1:1,000), anti-Ki67 (Dako, M7248, 1:500), anti-Tuj1 (Progenia, G7121, 1:1,000), anti-MAP2 (Abcam, ab32454, 1:1,000), anti-GFAP (Dako, Z0334, 1:1,000), anti-Nestin (Aves labs, NES, 1:500), anti-SOX2 (Millipore, MAB4343, 1:1,000), anti-MCM2 (Santa Cruz, sc-9839, 1:1,000). DyLight 680/800 conjugated secondary antibodies (Thermo Fisher Scientific) were used for Western blot. Alexa Fluor conjugated secondary antibodies (Invitrogen) were used for immunofluorescence staining. The following drugs were used: DAPT (Sigma-Aldrich), nocodazole (Sigma-Aldrich), colchicine (Sigma-Aldrich), roscovitine (Calbiochem), nimodipine (Sigma-Aldrich), Myr-CaMK IINtide (Calbiochem), STO-609 (Tocris), Bay K8644 (Calbiochem), Hesperadin (Selleckchem)

In vivo proliferation of NPCs in the adult hippocampus

Tissue processing and in vivo cell proliferation analysis were performed as previously described^{12,15}. Briefly, BrdU was dissolved in normal saline solution at a concentration of 10mg/ml, and filter sterilized. 8–9 weeks old mice received daily BrdU injections at the dose of 50mg/Kg body weight for 6 consecutive days, and were sacrificed for analysis 24 hours after the last (the 6th) BrdU injection. Stereological counting of the total number of BrdU or Ki67 labeled cells was performed under a Carl Zeiss Axioplan 2 Imaging microscope and the MBF Bioscience Stereo Investigator 8 software, using every 6th serial sections throughout the hippocampus. Scoring was performed without the knowledge of the genotype of the samples.

In vivo differentiation of NPCs in the adult hippocampus

Tissue processing and in vivo cell differentiation analysis were performed as previously described^{12,15}. Briefly, BrdU was dissolved in normal saline solution at a concentration of 10mg/ml, and filter sterilized. 8–9 weeks old mice received daily BrdU injections at the dose of 50mg/Kg body weight for 6 consecutive days, and were sacrificed for analysis 28 days after the last (the 6th) BrdU injection. Every 6th of the serial sections throughout the hippocampus were co-stained with an anti-BrdU antibody (to mark adult-born cells), an anti-NeuN antibody (to mark neurons), and an anti-S100 β antibody (to mark glial cells). Quantification was done using a confocal microscope (Nikon Eclipse E600, with Nikon EZ-C1 3.50 software) to first look for immunoreactivity of BrdU, and then switch to the other channels to check whether a given BrdU positive cell was also labeled by NeuN or S100 β . Cells were identified as neurons if they were positive for both BrdU and NeuN, as glial cells if they were positive for both BrdU and S100 β , or as undetermined if they were only positive for BrdU. All BrdU positive cells in the subgranular zone from all stained sections were included in the analysis. Percentage of each cell fate in each mouse was determined by dividing the number of cells from each cell fate by the total number of BrdU positive cells from the hippocampus of that mouse. Scoring was performed without the knowledge of the genotype of the samples.

Immunohistochemistry

10–12 weeks old mice were transcardially perfused with normal saline solution followed by 4% paraformaldehyde (PFA). Brains were carefully dissected out, post-fixed in 4% paraformaldehyde, cryoprotected in 30% sucrose, embedded and frozen in Tissue Tek. Serial coronal sections were cut at 40 μ m throughout the brain, and stained with appropriate primary and secondary antibodies.

Isolation and culture of adult NPCs

NPCs used in this study were isolated from the DG of 6 to 8-week-old male *Mecp2^{S421A;S424A}* mice and wild-type (WT) littermate controls based on published methods²⁷. Briefly, DG was microdissected from 400 μ m coronal sections of forebrain. After enzymatic digestion using MACS Neural Tissue Dissociation kit (Miltenyi Biotech), DMEM/F-12 (Invitrogen) containing 10% FBS (Invitrogen) were added into each sample for stopping digestion. After filtering through a 70- μ m cell strainer (BD Biosciences) and

washing with DMEM/F-12, the single-cell suspension was collected and cultured with proliferation medium: Neurobasal medium (Invitrogen) containing 20 ng/ml basic fibroblast growth factor (FGF-2, Waisman Biomanufacturing), 20 ng/ml epidermal growth factor (EGF, Peprotech), B27 supplement (Invitrogen), Penicillin Streptomycin (Invitrogen), and L-glutamine (Invitrogen) in a 5% CO₂ incubator at 37°C. Half of the medium was replaced every two days.

Proliferation and differentiation assays of adult NPCs

Proliferation and differentiation of aNPCs were analyzed using published method²⁸. Only early passage cells (between passage 4 and 10) and the same passage numbers of wild type and *Mecp2^{S421A:S424A}* cells were used for the assay. For each experiment, stereological counting (Stereo Investigator, MBF Bioscience) of immunofluorescence positive cells from duplicated wells were analyzed, and results were averaged as one data point (n = 1). At least 3 independent experiments (n = 3) were performed and used for statistical analyses for each analysis.

In cell proliferation assay, we dissociated aNPCs with 0.05% Trypsin-EDTA (Invitrogen) for no longer than 1 min, stopped the digest with Trypsin inhibitor (Sigma-Aldrich) and finally plated the cells on poly-L-lysine/laminin-coated cover slips at a density of 100,000 cells/well in proliferation medium (see above). At 20 h post-plating, 5 μM 5-bromo-2'-deoxyuridine (BrdU, Sigma-Aldrich) was added into the culture medium for 8 hours, after which the cells were fixed with 4% paraformaldehyde for 30 min at room temperature. To detect BrdU incorporation, fixed cells were pretreated with 1M HCl for 30 min at 37°C, and then washed with borate buffer, pH 8.5, for 30 min. We then followed our standard immunocytochemistry protocol.

For the differentiation assay, aNPCs were similar treated and plated as in the proliferation assay, but at a density of 50,000 cells/well. At 24 h post-plating, cells were changed into differentiation medium: Neurobasal medium with 1% B27 supplement, 1% Penicillin Streptomycin (Invitrogen), 2 mM L-glutamine (Invitrogen), 5 μM forskolin (Sigma-Aldrich), 1 μM retinoic acid (Sigma-Aldrich). Half of the medium was changed with fresh differentiation medium for four days, followed by fixation with 4% paraformaldehyde for 30 min and standard immunocytochemistry protocol.

Cell cycle analysis

Cells were fixed in 2% paraformaldehyde for 15min at room temperature, and stained with Propidium Iodide (PI) (50μg/ml) in the presence of RNase A (0.1mg/ml) for 40 min at 37°C and then overnight at 4°C. The stained cells were analyzed on a FACS Calibur (BD Biosciences).

Lentivirus preparation

HEK293 cells were triple transfected using the calcium phosphate method with the lentiviral expression plasmid pEF1α-NICD, pEF1α-GFP, LentiLox 3.7-shEGFP, or LentiLox 3.7-shAURKB and packaging vectors (pCAG-VSV-G and pCMV R8.91), and were switched to fresh media after 16 hours. The supernatants containing the viral particles were collected

48 hours after transfection and concentrated by ultracentrifuge (SW32 rotor, centrifuge at 25000 rpm, 4°C for 2.5 hours).

Transfection and co-immunoprecipitation

Neuro2A cells (ATCC CCL-131) were maintained in DMEM (Invitrogen). Transfection of EGFP, *Aurkb* and *Mecp2* expression plasmid was performed using Lipofectamine® LTX with Plus™ Reagent (Invitrogen). For co-immunoprecipitation, transfected cells were lysed with cell lysis buffer (50mM Tris-HCl, pH8.0, 170mM NaCl, 0.5% NP-40, protease inhibitor (Roche), Phosphatase inhibitor (Sigma-Aldrich)), following by sonication. Dynabeads (Invitrogen) were pre-washed with PBS/BSA (0.5% BSA in PBS) and incubated with antibody to form the beads/antibody complex. Protein lysis was then incubated with beads/antibody complex on a nutator at 4 °C over night. The beads were washed with lysis buffer for 3 times and finally boiled in Laemmli Sample Buffer (Bio-rad) with 0.5% 2-Mercaptoethanol at 95 °C for 10 minutes.

RNA extraction, qRT-PCR and Neural Stem Cell PCR Array

Total RNA was extracted from cultured adult NSCs using TRIzol Reagent (Invitrogen). The qScript™ cDNA SuperMix kit (Quanta Biosciences) was used for cDNA synthesis. Real-time quantitative PCR was performed on StepOne Plus Real-Time PCR System (Applied Biosystems) using iQ SYBR Green Supermix (Bio-rad). Fold change was calculated using the 2^{-Ct} method after normalization to Gapdh. For the sequences of all the qPCR primers used in this study, please see Supplementary Table 1. For microRNA expression, a 15- μ l reverse transcription reactions consisted of 5 ng of total RNA using TaqMan microRNA assay (mmu-miR-137 and snoRNA202) and Taqman MicroRNA Reverse Transcription Kit (Applied Biosystems) following the manufacturer's recommendations. Real-time PCR was performed in StepOne Plus Real-Time PCR System using TaqMan microRNA assay (mmu-miR-137 and snoRNA202) and TaqMan Universal PCR Master Mix, No AmpErase UNG (Applied Biosystems) following the manufacturer's recommendations. Relative level of miR-137 was calculated based on 2^{-Ct} method after normalization to the transcript level of snoRNA202 as the endogenous control. Neurogenesis and Neural Stem Cells PCR Array (Qiagen/SABiosciences, PAMM-404A, Version 3.0 system) was performed according to manufacturer's instruction. Data were analyzed using the online software from Qiagen/SABiosciences (<http://pcrdataanalysis.sabiosciences.com/pcr/arrayanalysis.php>).

Western blot analysis

Cultured adult NPCs were washed with PBS once and then lysed in Laemmli Sample Buffer (Bio-rad) with 0.5% 2-Mercaptoethanol at 95 °C for 10 minutes. Sonication was used to lyse the cells and shear the genomic DNA, before the samples were subjected to SDS-PAGE. The protein samples were then transferred to Protran BA 85 nitrocellulose membranes (Whatman). The membrane was blocked by 5% dry milk, and incubated with appropriate primary and DyLight dye-conjugated secondary antibodies. The Odyssey Western Detection Methods (LI-COR Biosciences) was used for signal detection. The integrated pixel intensity values for the target protein bands were analyzed with NIH ImageJ software, and then normalized to the intensity of the control β -Actin from the same samples.

Chromatin immunoprecipitation and gene-specific qPCR

Cultured aNPCs were crosslinked with 1% formaldehyde for 15 min. Crosslinking was stopped by adding 1/20 volume of 2.5M glycine. The following chromatin immunoprecipitation procedure was performed as previously described⁶. ChIP DNA and input DNA were dissolved in 20 μ l of nuclease free water and 1 μ l of DNA was used for each quantitative real-time PCR. Real-time quantitative PCR was performed on StepOne Plus Real-Time PCR System (Applied Biosystems) using iQ SYBR Green Supermix (Bio-rad). The ChIP DNA level was normalized to the input DNA level using the $2^{-\Delta\Delta C_t}$ method. Relative promoter occupancy was then calculated by setting the level of WT-MeCP2 binding as 1. Primers used in real time PCR are: Dll1-ChIP: 5'-gtgttgagcatgccatgagc-3' (forward) 5'-ctagctccaagaatcacacc-3' (reverse) Notch1-ChIP: 5'-tataggcatcaggaggattg-3' (forward) 5'-actcccttctacagaggctg-3' (reverse) Crh-ChIP: 5'-gtcaccaaggaggcgataccta-3' (forward) 5'-taaataataggccctgccaag-3' (reverse) Major Satellite-ChIP: 5'-catccacttgacgactgaaaa-3' (forward) 5'-gaggtccttcagtgtgattt-3' (reverse)

Endogenous co-immunoprecipitation

For co-immunoprecipitation, four 10cm plates of confluent grown NPCs were lysed in cell lysis buffer (50mM Tris-HCl, pH8.0, 170mM NaCl, 0.5% NP-40, protease inhibitor (Roche), Phosphatase inhibitor (Sigma-Aldrich)), following by sonication with a Bioruptor (Diagenode) for three 10-minute periods. Cells were continued lysed with rotation on a nutator at 4 °C for 30 minutes. Dynabeads (Invitrogen) were pre-washed with PBS/BSA (0.5% BSA in PBS) and incubated with antibody or IgG to form the beads/antibody complex. Protein lysate was then incubated with beads/antibody complex on a nutator at 4 °C over night. The beads were washed with lysis buffer for 3 times and finally boiled in Laemmli Sample Buffer (Bio-Rad) with 0.5% 2-Mercaptoethanol at 95 °C for 10 minutes.

In vitro kinase assay

0.5 μ g of Recombinant MeCP2 (Prospec, PRO-212) was incubated with AURKB-flag, AURKB-DN-flag or EGFP-flag, which were freshly immunopurified from 293T cells, in Kinase buffer (50mM HEPES, pH 7.5, 150mM NaCl, 10mM MgCl₂, 1mM DTT, protease inhibitor (Roche), Phosphatase inhibitor (Sigma-Aldrich)) with or without 100 μ M ATP at 30 °C for 30 minutes. The presence of phosphorylated S421 was detected by Western blot with anti-phospho-S421 antibody.

Statistical analysis

No statistical methods were used to predetermine sample sizes, but the samples sizes we used were consistent with those generally employed in the field. Data was first tested for normality using the D'Agostino-Pearson omnibus test when necessary. Comparisons between two groups were analyzed by unpaired t-test with Welch's correction. Multiple comparisons in the same data set were analyzed by one-way ANOVA followed by Tukey's multiple comparisons test. Data from multiple groups with multiple treatments were analyzed by two-way ANOVA followed by Tukey's multiple comparisons test. $P < 0.05$ was considered to be statistically significant. Statistical processing was performed using Microsoft Excel and GraphPad Prism Software.

Supplementary Material

Refer to Web version on PubMed Central for supplementary material.

Acknowledgments

We thank Shruti Marwaha and Fei Yu for assistance with mouse work, and Dr. Dan Bolt for assistance with statistical analysis. H.L. was supported by a pre-doctoral fellowship from the Stem Cell and Regenerative Medicine Center at the University of Wisconsin-Madison and a graduate student fellowship from the Friends of the Waisman Center. Q.C. was supported by a Young Investigator Award from NARSAD. This work was partially supported by grants from NICHD (R01 HD064743 and R21 HD066560 to Q.C. and P30 HD03352 to the Waisman Center), NIMH (R01 MH078972 and R01 MH080434 to X-Y.Z.), and the International Rett Syndrome Foundation (to P.J.).

References

1. Jaenisch R, Bird A. Epigenetic regulation of gene expression: how the genome integrates intrinsic and environmental signals. *Nat Genet.* 2003; 33 (Suppl):245–254. [PubMed: 12610534]
2. Amir RE, et al. Rett syndrome is caused by mutations in X-linked MECP2, encoding methyl-CpG-binding protein 2. *Nat Genet.* 1999; 23:185–188. [PubMed: 10508514]
3. Hagberg B. Rett's syndrome: prevalence and impact on progressive severe mental retardation in girls. *Acta Paediatr Scand.* 1985; 74:405–408. [PubMed: 4003065]
4. Chen WG, et al. Derepression of BDNF transcription involves calcium-dependent phosphorylation of MeCP2. *Science.* 2003; 302:885–889. [PubMed: 14593183]
5. Zhou Z, et al. Brain-specific phosphorylation of MeCP2 regulates activity-dependent Bdnf transcription, dendritic growth, and spine maturation. *Neuron.* 2006; 52:255–269. [PubMed: 17046689]
6. Li H, Zhong X, Chau KF, Williams EC, Chang Q. Loss of activity-induced phosphorylation of MeCP2 enhances synaptogenesis, LTP and spatial memory. *Nature neuroscience.* 2011; 14:1001–1008.10.1038/nn.2866 [PubMed: 21765426]
7. Cohen S, et al. Genome-Wide Activity-Dependent MeCP2 Phosphorylation Regulates Nervous System Development and Function. *Neuron.* 2011; 72:72–85.10.1016/j.neuron.2011.08.022 [PubMed: 21982370]
8. Zhong X, Li H, Chang Q. MeCP2 phosphorylation is required for modulating synaptic scaling through mGluR5. *The Journal of neuroscience : the official journal of the Society for Neuroscience.* 2012; 32:12841–12847.10.1523/JNEUROSCI.2784-12.2012 [PubMed: 22973007]
9. Deng JV, et al. MeCP2 in the nucleus accumbens contributes to neural and behavioral responses to psychostimulants. *Nature neuroscience.* 2010; 13:1128–1136.10.1038/nn.2614 [PubMed: 20711186]
10. Ma DK, et al. Epigenetic choreographers of neurogenesis in the adult mammalian brain. *Nature neuroscience.* 2010; 13:1338–1344.10.1038/nn.2672 [PubMed: 20975758]
11. Deng W, Aimone JB, Gage FH. New neurons and new memories: how does adult hippocampal neurogenesis affect learning and memory? *Nature reviews. Neuroscience.* 2010; 11:339–350.10.1038/nrn2822 [PubMed: 20354534]
12. Smrt RD, et al. Mecp2 deficiency leads to delayed maturation and altered gene expression in hippocampal neurons. *Neurobiol Dis.* 2007; 27:77–89. [PubMed: 17532643]
13. Szulwach KE, et al. Cross talk between microRNA and epigenetic regulation in adult neurogenesis. *J Cell Biol.* 2010; 189:127–141. [PubMed: 20368621]
14. Tsujimura K, Abematsu M, Kohyama J, Namihira M, Nakashima K. Neuronal differentiation of neural precursor cells is promoted by the methyl-CpG-binding protein MeCP2. *Exp Neurol.* 2009; 219:104–111.10.1016/j.expneurol.2009.05.001 [PubMed: 19427855]
15. Zhao X, et al. Mice lacking methyl-CpG binding protein 1 have deficits in adult neurogenesis and hippocampal function. *Proc Natl Acad Sci U S A.* 2003; 100:6777–6782. [PubMed: 12748381]

16. Leitch AE, Haslett C, Rossi AG. Cyclin-dependent kinase inhibitor drugs as potential novel anti-inflammatory and pro-resolution agents. *Br J Pharmacol.* 2009; 158:1004–1016.10.1111/j.1476-5381.2009.00402.x [PubMed: 19775281]
17. Bischoff JR, et al. A homologue of *Drosophila* aurora kinase is oncogenic and amplified in human colorectal cancers. *Embo J.* 1998; 17:3052–3065.10.1093/emboj/17.11.3052 [PubMed: 9606188]
18. Whittaker SR, et al. The cyclin-dependent kinase inhibitor seliciclib (R-roscovitine; CYC202) decreases the expression of mitotic control genes and prevents entry into mitosis. *Cell Cycle.* 2007; 6:3114–3131. [PubMed: 18075315]
19. Crosio C, et al. Mitotic phosphorylation of histone H3: spatio-temporal regulation by mammalian Aurora kinases. *Molecular and cellular biology.* 2002; 22:874–885. [PubMed: 11784863]
20. Selkoe D, Kopan R. Notch and Presenilin: regulated intramembrane proteolysis links development and degeneration. *Annual review of neuroscience.* 2003; 26:565–597.10.1146/annurev.neuro.26.041002.131334
21. Skene PJ, et al. Neuronal MeCP2 is expressed at near histone-octamer levels and globally alters the chromatin state. *Mol Cell.* 2010; 37:457–468. [PubMed: 20188665]
22. Jones PL, et al. Methylated DNA and MeCP2 recruit histone deacetylase to repress transcription. *Nat Genet.* 1998; 19:187–191. [PubMed: 9620779]
23. Ebert DH, et al. Activity-dependent phosphorylation of MeCP2 threonine 308 regulates interaction with NCoR. *Nature.* 2013; 499:341–345.10.1038/nature12348 [PubMed: 23770587]
24. Lyst MJ, et al. Rett syndrome mutations abolish the interaction of MeCP2 with the NCoR/SMRT co-repressor. *Nature neuroscience.* 2013; 16:898–902.10.1038/nn.3434 [PubMed: 23770565]
25. Baker SA, et al. An AT-hook domain in MeCP2 determines the clinical course of Rett syndrome and related disorders. *Cell.* 2013; 152:984–996.10.1016/j.cell.2013.01.038 [PubMed: 23452848]
26. Cheng TL, et al. MeCP2 Suppresses Nuclear MicroRNA Processing and Dendritic Growth by Regulating the DGCR8/Drosha Complex. *Dev Cell.* 2014; 28:547–560.10.1016/j.devcel.2014.01.032 [PubMed: 24636259]
27. Guo W, Patzlaff NE, Jobe EM, Zhao X. Isolation of multipotent neural stem or progenitor cells from both the dentate gyrus and subventricular zone of a single adult mouse. *Nature protocols.* 2012; 7:2005–2012.10.1038/nprot.2012.123 [PubMed: 23080272]
28. Guo W, et al. RNA-binding protein FXR2 regulates adult hippocampal neurogenesis by reducing Noggin expression. *Neuron.* 2011; 70:924–938.10.1016/j.neuron.2011.03.027 [PubMed: 21658585]

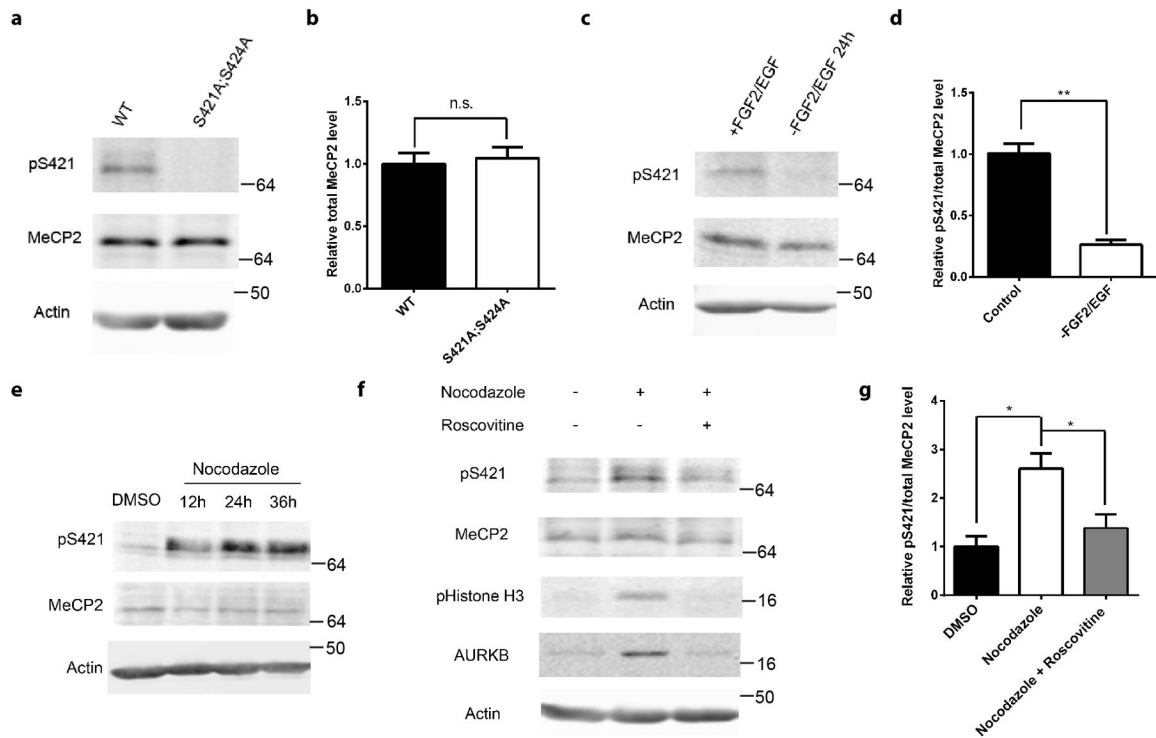


Figure 1. Phosphorylation of MeCP2 S421 is regulated by cell cycle in aNPCs

(a,b) Western blot analysis of MeCP2 S421 phosphorylation and the quantification of total MeCP2 protein level in WT and phosphor-mutant aNPCs. ($p=0.718$, unpaired t-test with Welch's correction, $n=3$ in each group) (c,d) Western blot analysis and quantification of the relative MeCP2 S421 phosphorylation level in WT aNPCs under normal proliferating condition and FGF2/EGF withdrawal for 24 hours. ($n=3$ in each group) (e) Western blot analysis reveals that MeCP2 S421 phosphorylation is induced by synchronizing aNPCs with nocodazole (150ng/ml). (f,g) Western blot analysis and quantification of the relative MeCP2 S421 phosphorylation level in aNPCs under conditions: 1) DMSO, 2) 36 hours of nocodazole treatment, 3) 24 hours of roscovitine (25 μ M) treatment after pre-synchronization of the cells by nocodazole for 12 hours. ($n=3$ in each group) Numbers next to Western blots are molecular weight markers. The bar graph shows the mean \pm s.e.m * $p<0.05$ ** $p<0.01$

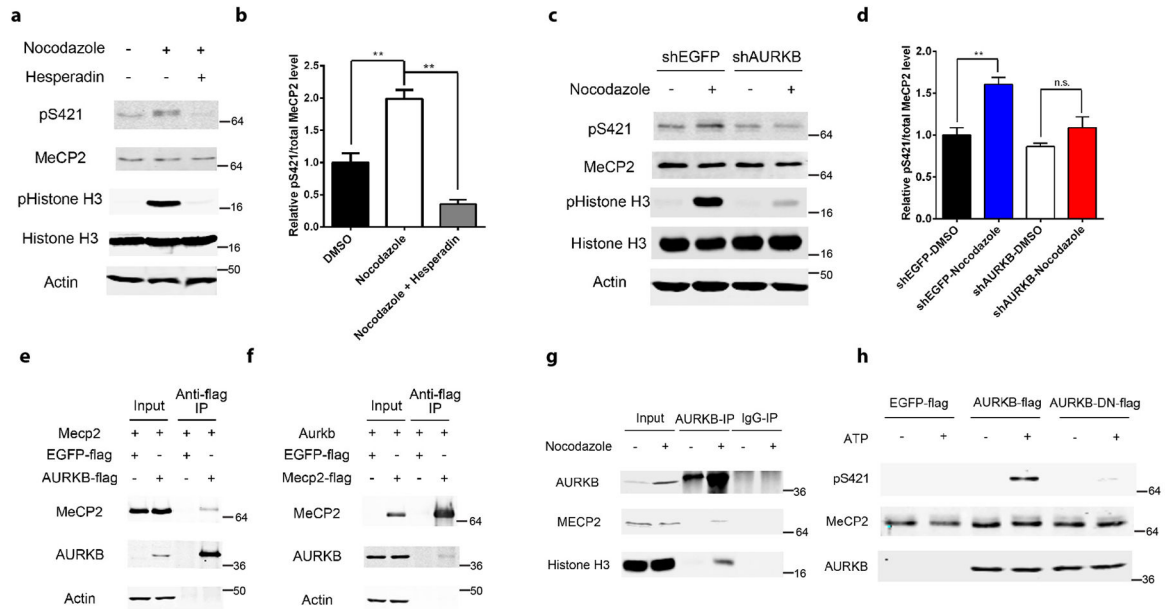


Figure 2. Aurora kinase B is required for MeCP2 S421 phosphorylation in the aNPCs
(a,b) Western blot analysis and quantification of the relative MeCP2 S421 phosphorylation level in aNPCs: 1) DMSO, 2) 36 hours of nocodazole (150ng/ml) treatment, 3) 24 hours of hesperadin (2 μ M) treatment after pre-synchronization of the cells by nocodazole for 12 hours. (n=3 in each group) **(c,d)** Western blot analysis and quantification of the relative MeCP2 S421 phosphorylation level in EGFP-shRNA or AURKB-shRNA lentivirus infected aNPCs, which are treated with DMSO or nocodazole for 24 hours. **(e,f)** Western blot analysis reveals that MeCP2 and AURKB are co-immunoprecipitated reciprocally. **(g)** Western blot analysis reveals endogenous interaction between MeCP2 and AURKB in aNPCs. **(h)** In vitro kinase assay followed by Western blot demonstrates that AURKB can phosphorylate S421 on MeCP2. Numbers next to Western blots are molecular weight markers.

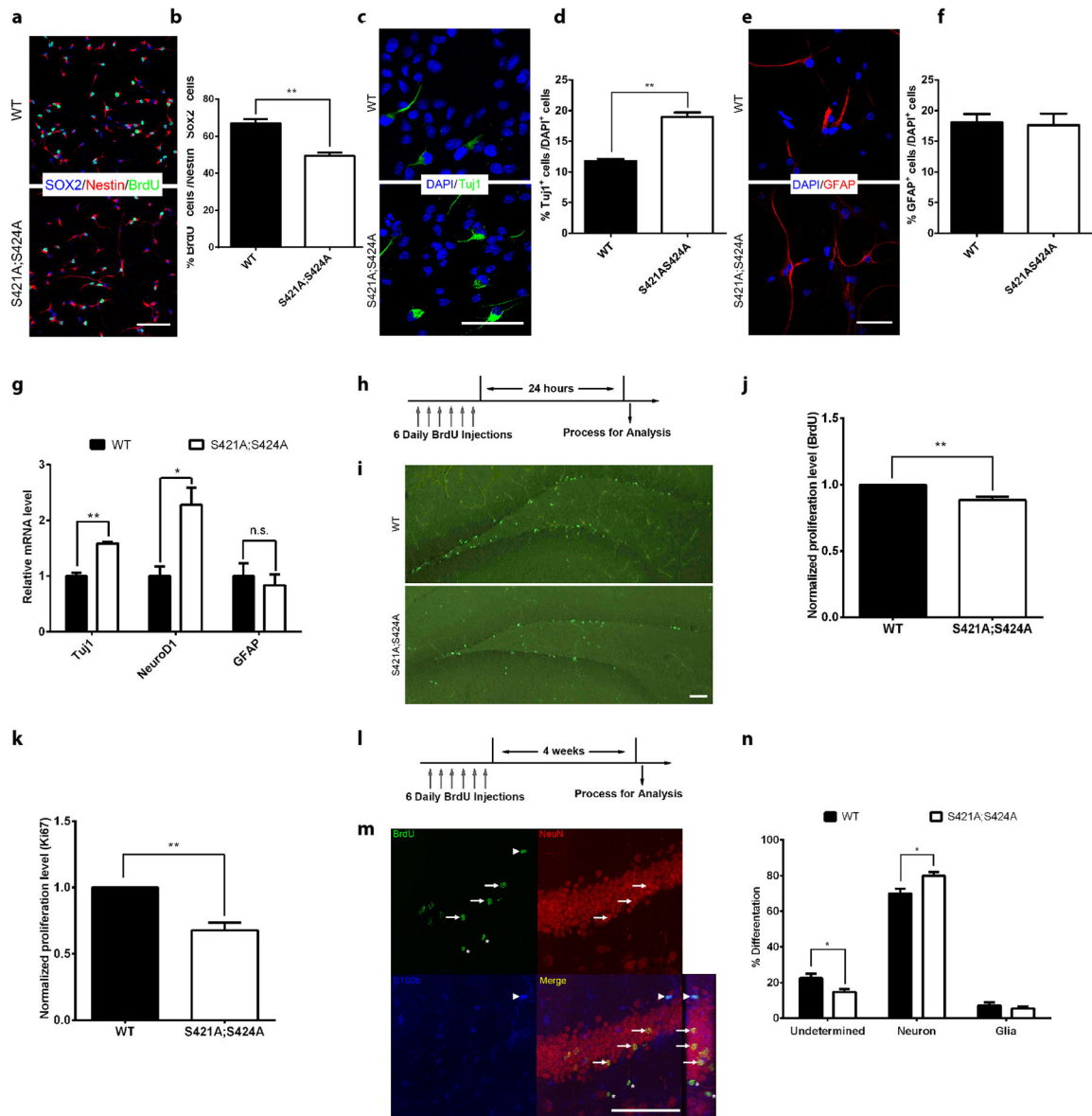


Figure 3. Altered proliferation and differentiation of MeCP2 phosphor-mutant aNPC *in vitro* and *in vivo*

(a) Representative images of aNPCs isolated from WT and *Mecp2*^{S421A;S424A/y} hippocampus with BrdU pulse labeling, followed by immunocytochemistry analysis (b) Quantification of the percentage of BrdU/Sox2/Nestin triple-labeled cells in WT and *Mecp2*^{S421A;S424A/y} aNPCs. (n=3 in each group) (c) Representative images of Tuj1+ neurons differentiated from WT and *Mecp2*^{S421A;S424A/y} aNPCs (d) Quantification of the percentage of Tuj1+ cells in WT and *Mecp2*^{S421A;S424A/y} aNPCs upon differentiation. (n=3 in each group) (e) Representative images of GFAP+ astrocyte differentiated from WT and *Mecp2*^{S421A;S424A/y} aNPCs (f) Quantification of the percentage of GFAP+ cells in WT and *Mecp2*^{S421A;S424A/y} aNPCs upon differentiation. (n=3 in each group) (g) Relative mRNA level of neuronal marker (*Tuj1* and *NeuroD1*) and astrocyte marker (*GFAP*) in WT and *Mecp2*^{S421A;S424A/y}

aNPCs upon differentiation, assayed by RT-qPCR. (n=3 in each group) **(h)** Schematics of the design of the *in vivo* BrdU labeling experiment. **(i)** Representative images of WT and the *Mecp2^{S421A;S424A/y}* brain sections stained for BrdU immunoreactivity. **(j)** Quantification of relative number of BrdU+ cells obtained through stereological counting from WT and *Mecp2^{S421A;S424A/y}* mice (n=9 in each group). **(k)** Quantification of the relative number of Ki67+ cells obtained through stereological counting from WT and *Mecp2^{S421A;S424A/y}* mice (n=6 in each group). **(l)** Schematics of the design of *in vivo* BrdU pulse/chase experiment to examine the differentiation profile of the adult-born hippocampal cells. **(m)** Representative confocal microscopy images to demonstrate how each cell type is identified. Three adult-born neurons (co-stained by BrdU and NeuN) are marked by arrow. One adult-born glial cell (co-stained by BrdU and S100b) is marked by arrowhead. Two adult-born undetermined cells (stained by BrdU only) are marked by asterisk. The rectangle panel to the right of the merged channel image is the y-z view of the same optical stack. The optical size of the z-scan is 0.4µm/step. **(n)** Quantification of proportions of the cell fate choices made by the dividing aNPCs in the hippocampus of WT and *Mecp2^{S421A;S424A/y}* mice. All scale bars are 50 µm. The bar graph shows the mean ± s.e.m * p<0.05 ** p<0.01

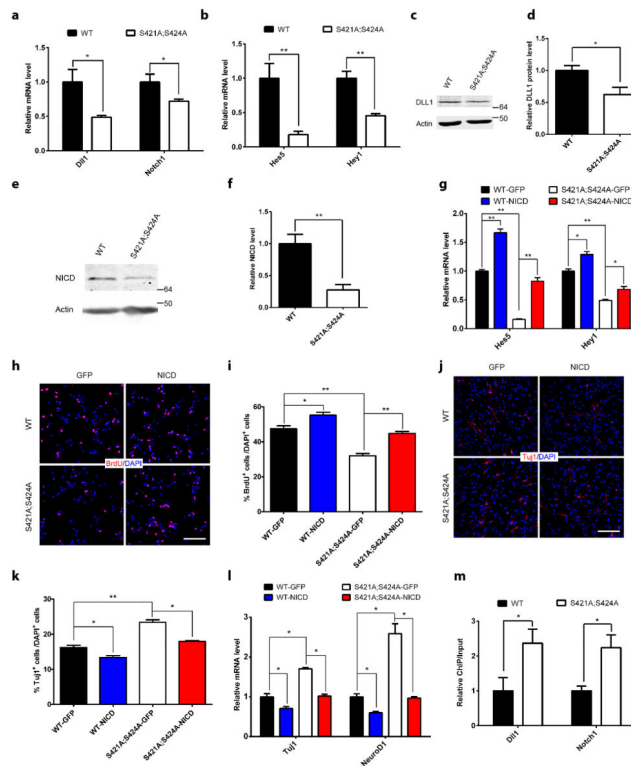


Figure 4. Reduced Notch signaling in MecP2 phosphor-mutant aNPCs and phenotypic rescue by NICD overexpression

(a) RT-qPCR analysis of the relative mRNA level of *Dll1* and *Notch1* in WT and *Mecp2*^{S421A;S424A/y} aNPCs. (n=5 in each group for *Dll1*, n=8 in each group for *Notch1*) (b) RT-qPCR analysis of the relative mRNA level of Notch target gene *Hes5* and *Hey1* in WT and *Mecp2*^{S421A;S424A/y} aNPCs. (n=5 in each group) (c,d) Western blot analysis and quantification of the relative protein level of DLL1 in WT and *Mecp2*^{S421A;S424A/y} aNPCs. (n=4 in each group) (e, f) Western blot analysis and quantification of NICD level in WT and *Mecp2*^{S421A;S424A/y} aNPCs (n=5 in each group) (g) RT-qPCR analysis of the relative mRNA level of *Hes5* and *Hey1* in WT and *Mecp2*^{S421A;S424A/y} aNPCs infected with GFP- or NICD-lentivirus. (n=3 in each group) (h, i) Representative images and quantification of BrdU-labeled cells in WT and *Mecp2*^{S421A;S424A/y} aNPCs infected with GFP- or NICD-lentivirus, followed by BrdU pulse labeling. (n=3 in each group) (j, k) Representative images and quantification of Tuj1+ neurons differentiated from WT and *Mecp2*^{S421A;S424A/y} aNPCs infected with GFP- or NICD-lentivirus. (n=3 in each group) (l) Relative mRNA level of neuronal marker (*Tuj1* and *NeuroD1*) and astrocyte marker (*GFAP*) in WT and *Mecp2*^{S421A;S424A/y} aNPCs, which are infected with GFP- or NICD-lentivirus and then cultured in differentiation condition. (n=3 in each group) Scale bar 50 μ m. (m) ChIP-qPCR analysis of the promoter occupancy of WT and phosphor-mutant MeCP2 on *Dll1* and *Notch1* promoters. (n=4 in each group) Numbers next to Western blots are molecular weight markers. The bar graphs in this figure show the mean \pm s.e.m * p<0.05 ** p<0.01